Environmental Science & Technology

Article

pubs.acs.org/est

Estimation of Groundwater Radon in North Carolina Using Land Use Regression and Bayesian Maximum Entropy

Kyle P. Messier,[*,†] Ted Campbell,[‡] Philip J. Bradley,[§] and Marc L. Serre[†]

[†]Department of Environmental Science and Engineering, Gillings School of Global Public Health, University of North Carolina, Chapel Hill, North Carolina 27599, United States

[‡]Division of Water Resources, North Carolina Department of Environment and Natural Resources, 2090 U.S. 70 Highway, Swannanoa, North Carolina 28778, United States

[§]North Carolina Geological Survey, Division of Energy, Mineral, and Land Resources - North Carolina Department of Environment and Natural Resources, 1612 Mail Service Center, Raleigh, North Carolina 27699, United States

Supporting Information

ABSTRACT: Radon (^{222}Rn) is a naturally occurring chemically inert, colorless, and odorless radioactive gas produced from the decay of uranium (^{238}U), which is ubiquitous in rocks and soils worldwide. Exposure to ^{222}Rn is likely the second leading cause of lung cancer after cigarette smoking via inhalation; however, exposure through untreated groundwater is also a contributing factor to both inhalation and ingestion routes. A land use regression (LUR) model for groundwater ^{222}Rn with anisotropic geological and ^{238}U based explanatory variables is developed, which helps elucidate the factors contributing to elevated ^{222}Rn across North Carolina. The LUR is also integrated into the Bayesian Maximum Entropy (BME) geostatistical framework to increase accuracy and produce a point-level LUR-BME model of groundwater ^{222}Rn across North Carolina including prediction uncertainty. The LUR-BME model of groundwater ^{222}Rn results in a leave-one out cross-validation r^2 of 0.46 (Pearson correlation coefficient = 0.68), effectively predicting within the spatial covariance range. Modeled results of ^{222}Rn concentrations show variability among intrusive felsic geological formations likely due to average bedrock ^{238}U defined on the basis of overlying stream-sediment ^{238}U concentrations that is a widely distributed consistently analyzed point-source data.

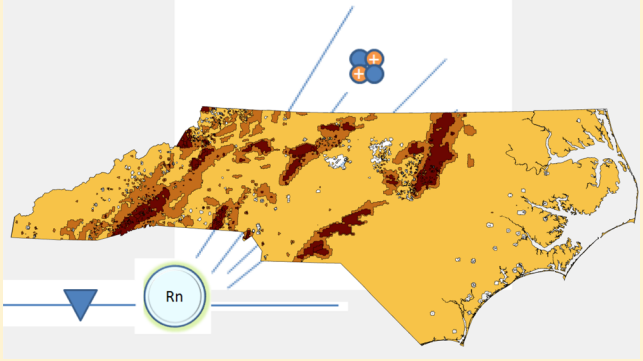

1. INTRODUCTION

Radon (^{222}Rn) is a naturally occurring chemically inert, colorless, and odorless radioactive gas[1] produced from the decay of uranium (^{238}U), which is ubiquitous in rocks and soils worldwide. Outdoor air ^{222}Rn levels are generally very low (<1 pCi/L, <0.037 Bq/L); however, when ^{222}Rn enters a residential home, through accumulation its concentration can increase to levels that may lead to increased health risks.[1] There is vast literature supporting the conclusion that exposures via inhalation of indoor air contaminated with radon lead to a significantly increased risk of lung cancer morbidity in both never-smokers and smokers.[2−7] Exposure to ^{222}Rn is likely the second leading cause of lung cancer after smoking in the US.[4,8,9] Important routes of inhalation exposure result from ^{222}Rn gas directly escaping from soil and rock and accumulating in the indoor environment; however, ^{222}Rn can also degas from untreated groundwater used for showering, dishwashing, and clothes washing resulting in exposures in direct vicinity to the breathing zone.[10,11]

^{222}Rn in groundwater is not only a concern because of its contribution to indoor air ^{222}Rn but also due to the direct ingestion of drinking water with elevated ^{222}Rn. There is evidence that exposure to ^{222}Rn through drinking water and indoor air can lead to increased risk of stomach cancer;[8,12] however, this human health end point is understudied compared to lung cancer and there is not a consensus on the extent of the risk.[4]

The association between groundwater ^{222}Rn and underlying geological formations has been shown in many previous studies. Brutsaert et al.[13] found positive associations between ^{222}Rn and granites, metamorphic rocks, and other chemical parameters in Maine, USA, through graphical and tabular comparison of measured values. Further solidifying this relationship, Yang et al.[14] showed increased risk for elevated ^{222}Rn within a 5 km distance to granitic intrusions in Maine, USA, using the nonparametric Kruskal−Wallis one-way analysis of variance (ANOVA). Likewise, associations between elevated ^{222}Rn and granites and granitic gneisses have been shown in North

Received: March 24, 2015
Revised: July 15, 2015
Accepted: July 20, 2015
Published: July 20, 2015

DOI: 10.1021/acs.est.5b01503
Environ. Sci. Technol. 2015, 49, 9817−9825

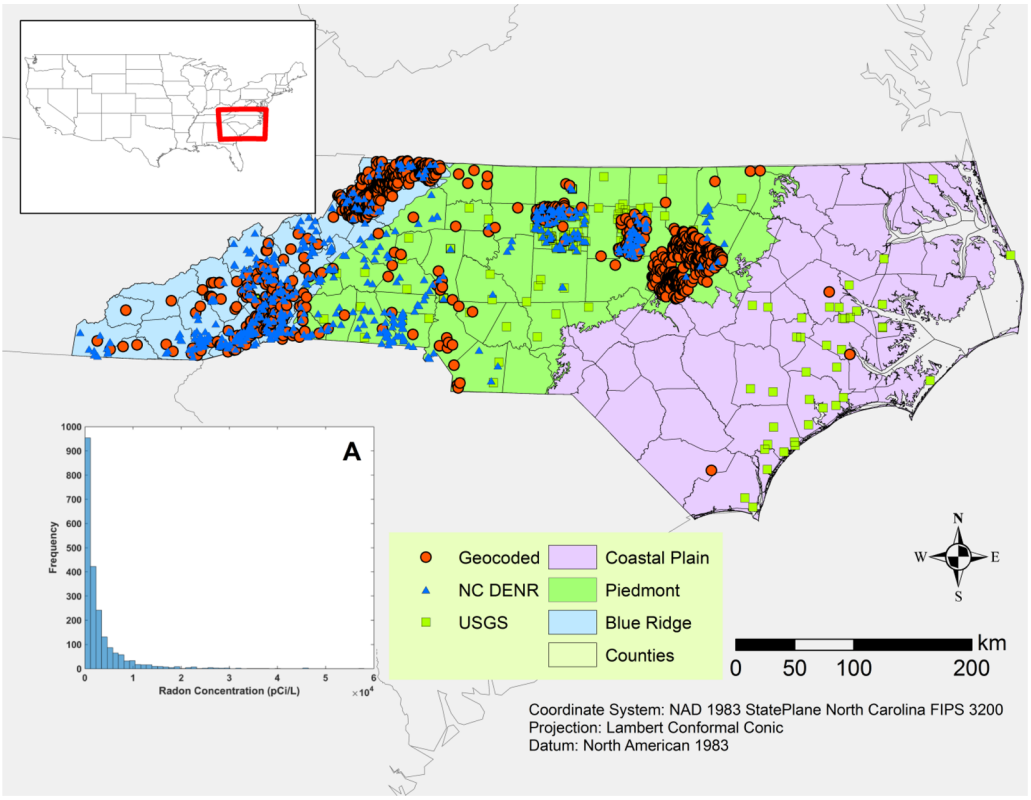

Figure 1. Radon data source spatial distribution detailed by its source. The three physiographic regions of North Carolina are detailed by color: Coastal Plain is light pink, Piedmont is green, and Blue Ridge is light blue. (A) Frequency histogram of the radon data. Note its log-normal distribution and the "$\times 10^4$" multiplier on the x-axis label (e.g., 2×10^4 pCi/L).

Carolina.[15,16] Prediction of groundwater ^{222}Rn on medium to large area scales (>10^0 km) has been implemented with Kriging models[17] and multivariate statistics accounting for ^{238}U concentration and geology independently;[18] however, their models did not account for potential geochemical and geologic interactions.

Previous studies have also attempted to find associations and make predictions of groundwater ^{222}Rn based on ^{238}U and other hydrogeochemical parameters such as alkalinity and conductivity. Yang et al.[14] observed weak, but positive, correlations at intermediate scales (10^0–10^1 km) between ^{238}U and ^{222}Rn in granitic bedrock aquifers of Maine, USA. Salih et al.[19] used Co-Kriging with ^{238}U as the secondary variable to map groundwater ^{222}Rn in southeast Sweden, which produced good predictions at unmonitored locations, but had weak correlation with ^{238}U ($R^2 < 0.1$).

About 25% of the Piedmont and Blue Ridge physiographic regions of North Carolina are underlain with rocks commonly associated with elevated ^{222}Rn in water, namely felsic intrusive rocks such as granites and granitic gneisses. Through water sampling Campbell et al.[16] have found 19 counties in North Carolina that are particularly susceptible to elevated radon in water. In this study, we use the samples from Campbell et al.[16] plus geocoded samples from private well sources and USGS to model the groundwater ^{222}Rn concentrations across North Carolina.

Several counties in western North Carolina are classified as EPA zone 1 counties, with predicted indoor air ^{222}Rn concentrations above the action level of 4 picocuries per liter (pCi/L; 0.15 Bq/L).[20,21] Over 90% of wells sampled in that region exceed the EPA's proposed maximum contaminant level of 300 (11.1) pCi/L (Bq/L), and a large number exceeded the alternate MCL of 4000 (148) pCi/L (Bq/L).[16] Since monitoring ^{222}Rn concentration is not mandatory for private well owners,[22] elucidating the spatial distribution of radon across the state is indispensable to inform the public about exposure to waterborne ^{222}Rn. Moreover, since North Carolina has on average 1/3 of each county population relying on untreated groundwater as its drinking water source,[23] quantifying potential exposures is important. Furthermore, the proportion of the population potentially exposed in North Carolina is significantly higher than the United States average.[16,20]

Land use regression (LUR)[24−29] modeling is a proven method that complements monitoring programs and provides effective means for water quality exposure assessments. Bayesian Maximum Entropy (BME) is a modern spatiotemporal geostatistical framework for incorporating measurements as well as various knowledge bases in a logical and theoretically sound manner to produce estimates of variables of interest at unmonitored locations.[30] It has been shown to successfully estimate groundwater quality distributions of contaminants.[28,31,32] An advantage of BME over purely spatial linear geostatistical approaches is its ability to quantify spatial and temporal variability, which is then used in the estimation process at unmonitored locations. BME, like all geostatistical methods, is data driven and can only provide reliable estimates within the vicinity of measured values; however, BME provides a sound framework to combine multiple sources of data. This has been successfully demonstrated with incorporation of deterministic mean trend functions, such as a LUR model, into BME for groundwater contaminants.[28,32]

DOI: 10.1021/acs.est.5b01503
Environ. Sci. Technol. 2015, 49, 9817−9825

The objectives of this study are to (1) develop a linear anisotropic LUR model for point-level groundwater ^{222}Rn in North Carolina, (2) integrate the LUR model into BME to produce the first model for point-level groundwater ^{222}Rn that fully quantifies its distribution with a mean or median and error variance, and (3) elucidate and develop hypotheses about geological and hydrogeochemical factors associated with groundwater ^{222}Rn and generalizable for easier extrapolation to additional areas. To these ends, we create groundwater ^{222}Rn explanatory variables based on the recent published geological and accompanying GIS information[33] and stream sediment and groundwater ^{238}U data.[34] Results are of interest to a range of stakeholders including (1) agencies that regulate drinking-water sources or that monitor health outcomes from ingestion of drinking-water, (2) agencies that monitor ^{222}Rn and provide remediation options to homeowners with increased risk of elevated radon, (3) builders and development planners, (4) geologists and hydrogeologists interested in environmental and human health applications of geological surveys, and (5) well owners and the general public.

2. METHODS

2.1. Radon Data and Spatial Explanatory Variables. Groundwater ^{222}Rn data[35,36] (Figure 1) were obtained from state agencies and private companies to form a database with over 2000 observations across North Carolina. Details on the data sources are available in the Supporting Information.

Spatial explanatory variables representing the underlying geology were calculated prior to model development. For a given geology feature, the corresponding geological variable was calculated as the percentage of that geological feature within an elliptical buffer centered on each radon measurement. All of the explanatory variables have an inherent spatial distance parameter, which hereinafter is referred to as the *hyperparameter*.[28,37] Each geological variable is characterized by a set of *ellipse hyperparameters* and its *geological classification scale*, as follows:

(i). Ellipse Hyperparameters. The ellipse buffer used to calculate the percent of a given geological feature captures the anisotropy and spatial range of the corresponding geological formation of interest. A given ellipse is defined using a set $\mathbf{\Lambda} = (\lambda_1, \lambda_2, \phi)$ of three ellipse hyperpameters which are the major and minor ellipse buffer radii λ_1 and λ_2, respectively, and the angle ϕ of ellipse rotation with respect to the horizontal axis. Each variable is calculated with multiple hyperparameter values since these are unknown a priori. In the final model selection process a maximum of one ellipse hyperparameter set $\mathbf{\Lambda}$ is allowed to be selected for each geological variable to avoid multicollinearity and effectively optimize the hyperparameters. The ellipse axis lengths included in this study are 1000, 2500, 5000, 7500, 10 000 m. The ellipse angles of rotation included are 0°, 45°, 90°, and 135°.

(ii). Geological Classification Scale. Geological features are defined at three different geological spatial scales, which are natural to lithological descriptions of geology and allow the model to distinguish between large area and small area effects of geology on groundwater ^{222}Rn. The most general and largest area scale is referred to as *General Geological Descriptions* (subsequently referred to as general), and this includes classifications such as intrusive felsic, intrusive mafic, and orthogneiss. These large area scale descriptions are subdivided into intermediate scale geologic descriptions referred to as *Lithotectonic Element* (subsequently referred to as element), which are themselves subdivided into the most detailed geologic descriptions referred to as *units*. Maps and details of the geological classification at each scale are available in the Supporting Information. These geological classifications are based on the underlying geology provided by Hibbard et al.[33] The provided GIS attributes by Hibbard et al. were enhanced with North Carolina-centric names based on North Carolina Geological Survey information for interpretability; however, the actual extent of each geological feature remains unchanged.

For a given ellipsoid and geological feature, we define the *geology percent variable*, as well as several corresponding *geology and uranium variables*, as follows:

(i). Geology Percent Variable. The percent $G^{(l)}(\boldsymbol{s};\ \mathbf{\Lambda})$ of geological feature (l) within an ellipse $(\boldsymbol{s}, \mathbf{\Lambda})$ centered at spatial location $\boldsymbol{s}$ and with hyperparameter set $\mathbf{\Lambda}$ is calculated as

$$G^{(l)}(\mathbf{s};\ \mathbf{\Lambda}) = \frac{1}{n_i(\mathbf{\Lambda})} \sum_{j=1}^{n_i(\mathbf{\Lambda})} I_j^{(l)}(\mathbf{s};\ \mathbf{\Lambda}) \tag{1}$$

where $I_j^{(l)}$ is an indicator representing the presence/absence of geological feature (l) at the jth pixel in the ellipse and n_i is the total number of pixels within the ellipse.

(2). Geology and Uranium Variables. For each stand-alone geological percent variable we define several corresponding geology and uranium variables that combine geological information with uranium information obtained from the National Uranium Resource Evaluation (NURE) Hydrogeochemical and Stream Sediment Reconnaissance[34] data, which are widely distributed consistently analyzed point-source data intending to represent average bedrock ^{238}U.[38] The geology and uranium variable $H_j^{(l)}(\boldsymbol{s};\ \mathbf{\Lambda})$ is calculated for geological feature (l) within the ellipse $(\boldsymbol{s}, \mathbf{\Lambda})$ as the product of the geological percent variable $G_i^{(l)}(\boldsymbol{s};\ \mathbf{\Lambda})$ times the average uranium, or normalized uranium concentration, in that geological feature within the ellipse, i.e.

$$H^{(l)}(\mathbf{s};\ \mathbf{\Lambda}) = G^{(l)}(\mathbf{s};\ \mathbf{\Lambda}) \left(\frac{1}{m_i(\mathbf{s};\ \mathbf{\Lambda})} \sum_{j=1}^{m_i(\mathbf{s};\mathbf{\Lambda})} U_j^{(l)}(\mathbf{s};\ \mathbf{\Lambda}) \right) \tag{2}$$

where $U_j^{(l)}(\boldsymbol{s};\ \mathbf{\Lambda})$ is the concentration of ^{238}U in the groundwater or stream sediment, or the ^{238}U centration normalized by alkalinity, or ^{238}U normalized by conductivity, at the jth grid cell in the ellipse $(\boldsymbol{s};\ \mathbf{\Lambda})$ that contains geology (l), and $m_i\ (\boldsymbol{s};\ \mathbf{\Lambda})$ is the number of raster data grid cells for geology (l) in the ellipse $(\boldsymbol{s};\ \mathbf{\Lambda})$. ^{238}U normalized variables are included as potential variables because they help remove ^{238}U anomalies,[39,40] and stream sediment variables are included because ^{238}U solubility and groundwater flow results in its accumulation near streams. A summary description of the variables is available in the Supporting Information (Table S1). The details of eqs 1 and 2 are aided by Figure 2, which shows an example of the total area within an ellipse, $n(\mathbf{\Lambda})$, and a geological formation of interest, $m(\boldsymbol{s};\ \mathbf{\Lambda})$, within the ellipse.

2.2. Land Use Regression and Model Selection. We implement a linear land use regression (LUR) model for ^{222}Rn concentration as follows:

$$Y_i = \beta_0 + \sum_{l=1}^{L} \beta_l X_i^{(l)}(\mathbf{\Lambda}_l) + \varepsilon_i \tag{3}$$

where Y_i is the log-transform of ^{222}Rn concentration at point i, $X_i^{(l)}(\mathbf{\Lambda}_l)$ is the lth source predictor variable at point i with

DOI: 10.1021/acs.est.5b01503
Environ. Sci. Technol. 2015, 49, 9817−9825

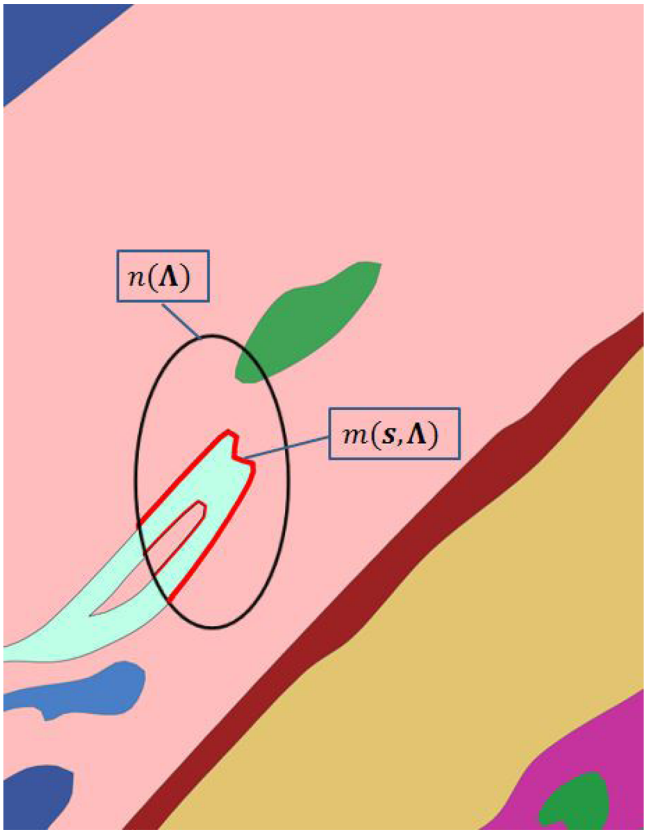

Figure 2. Number of cells in ellipse ($\boldsymbol{s}$; $\boldsymbol{\Lambda}$) $n(\boldsymbol{\Lambda})$ (black line) located at $\boldsymbol{s}$ and with hyperparameters $\boldsymbol{\Lambda}$ and number of cells in the geology of interest (red line) in the ellipse $\boldsymbol{m}(\boldsymbol{s}, \boldsymbol{\Lambda})$. In this example, the light blue represents the geological formation of interest, and $\boldsymbol{m}(\boldsymbol{s}, \boldsymbol{\Lambda})$ corresponds to the area outlined in red.

hyperparameter set $\boldsymbol{\Lambda}_l$, β_l is its source regression coefficient, and ε_i is an error term.

Variables are selected through a modified stepwise regression procedure for LUR models with multiple hyperparameter values called *a distance decay regression selection strategy* (ADDRESS).[25] Variables selected through ADDRESS provide evidence about the scale (i.e., general, elements, unit) and geochemical factors associated with elevated ^{222}Rn. To be more physically meaningful, all variables are considered source terms and are constrained to be positive. This model formulation supports the hypothesis that regions of elevated ^{222}Rn, or "hot spots", are due to the underlying geology and ^{238}U and that, while certain geological formations are associated with low ^{222}Rn, geological formations do not physically decrease the amount of ^{222}Rn.

2.3. BME Estimation Framework for Space/Time Mapping Analysis. To improve estimation accuracy, we integrate the time-averaged LUR results into the Bayesian Maximum Entropy (BME) method of modern spatiotemporal geostatistics.[41,42] We only provide the fundamental BME equations for mapping ^{222}Rn. The reader is referred to other works for more detailed derivations of BME equations[41,43] and the LUR integration into BME.[28]

Let $Z(\boldsymbol{p})$ be the space/time random field (S/TRF) describing the distribution of groundwater log-^{222}Rn across space and time, where $\boldsymbol{p} = (\boldsymbol{s}, t)$, $\boldsymbol{s}$ is the space coordinate, and t is time. The knowledge available is organized in the general knowledge base (G-KB) about the space/time trend and variability (e.g., mean, covariance) of ^{222}Rn across the study domain, and the site-specific knowledge base (S-KB) corresponding to the hard and soft data $\boldsymbol{z}_d$ available at a set of specific space/time points $\boldsymbol{p}_d$.

First, we define the transformation of log-^{222}Rn data $\boldsymbol{z}_d$ at locations $\boldsymbol{p}_d$ as

$$\boldsymbol{x}_h = \boldsymbol{z}_h - o_Z(\boldsymbol{p}_h) \tag{4}$$

where $o_Z(\boldsymbol{p}_h)$ may be any deterministic offset that can be mathematically calculated at any space/time coordinate $\boldsymbol{p}$. We then define $X(\boldsymbol{p})$ as a homogeneous/stationary S/TRF representing the variability and uncertainty with the transformed data $\boldsymbol{x}_d$, i.e. such that $\boldsymbol{x}_d$ is a realization of $X(\boldsymbol{p})$. Finally we let $Z(\boldsymbol{p}) = X(\boldsymbol{p}) + o_Z(\boldsymbol{p})$ be the S/TRF representing groundwater log-^{222}Rn. In this study, we consider two choices for $o_Z(\boldsymbol{p})$: (1) a constant value determined by the statewide log-^{222}Rn mean resulting in a purely BME model and (2) the LUR estimate, notated as $\boldsymbol{L}_z(\boldsymbol{p}_h)$, resulting in a LUR-BME model.

The G-KB for the S/TRF $X(\boldsymbol{p})$ describes its local space/time trends and dependencies. In this work, the general knowledge consists of the space/time mean trend function $m_x(\boldsymbol{p}) = E[X(\boldsymbol{p})]$ and the covariance function $C_X(\boldsymbol{p}, \boldsymbol{p}') = E[[X(\boldsymbol{p}) - m_x(\boldsymbol{p})][X(\boldsymbol{p}') - m_x(\boldsymbol{p}')]]$ of the S/TRF $X(\boldsymbol{p})$. We calculate isotropic and anisotropic experimental covariance values at four directions of azimuth (0, 45, 90, 135). Additionally, we divide the BME and LUR-BME analysis into three physiographic regions (Figure 1) of North Carolina based on geological properties: Blue Ridge, Piedmont, and Coastal Plain. The covariance is modeled by physiographic region if there are significant differences in model parameters between each region. Furthermore, the principal anisotropic axis is determined by examination of the experimental covariance plots and the major axis of an ellipse fit to a rose diagram: a plot of the spatial experimental covariance range as a function of the azimuth. For anisotropic models, the range of the covariance is always the range of the model along the principal axis and coordinates are converted from the anisotropic to isotropic case to produce a single data and coordinate set that accounts for the anisotropy.

S-KB consists of hard data and soft data; with hard data, $\boldsymbol{x}_h = \boldsymbol{z}_h - \boldsymbol{L}_z(\boldsymbol{p}_h)$, for data points where $\boldsymbol{z}_h$ is observed over the detection limit and soft data, $\boldsymbol{X}_s$, is at locations $\boldsymbol{p}_s$ where ^{222}Rn is observed below the detection limit. Following the work of Messier et al.,[28,32] the BME soft data for log-^{222}Rn, $f_s(.)$, is modeled as a Gaussian distribution truncated above the log of the detection limit.

The overall knowledge bases considered consist of $G = \{m_x(\boldsymbol{p}), C_X(\boldsymbol{p}, \boldsymbol{p}')\}$ and $S = \{f_s(.), \boldsymbol{X}_h\}$. In this case the BME set of equations reduces to

$$f_K(x_k) = A^{-1} \int d\boldsymbol{x}_s f_G(\boldsymbol{x}_h, \boldsymbol{x}_s, x_k) f_S(\boldsymbol{x}_s) \tag{5}$$

where $f_K(x_k)$ is the BME posterior probability distribution function (PDF) estimate for the offset-removed log-^{222}Rn(x_k) at some unmonitored estimation point $\boldsymbol{p}_k$, $f_G(\boldsymbol{x}_h, \boldsymbol{x}_s, x_k)$ is the multivariate Gaussian PDF for $(\boldsymbol{x}_h, \boldsymbol{x}_s, x_k)$ with mean and variance-covariance given by G-KB, $f_S(\boldsymbol{x}_s)$ is the truncated Gaussian PDF of $\boldsymbol{X}_s$, and A^{-1} is a normalization constant. After the BME analysis is conducted, $o_Z(\boldsymbol{p})$ is added back to obtain log-^{222}Rn concentrations.

2.4. Validation Statistics. Results between LUR, BME, and LUR-BME are compared with a leave-one-out cross-

DOI: 10.1021/acs.est.5b01503
Environ. Sci. Technol. 2015, 49, 9817−9825

Table 1. Land Use Regression Model Selected through ADDRESS

variable	geological scale	chemistry/percent	ellipse (major, minor, angle)	beta	*p*-value
intercept				6.0829	0
intrusive felsic	general	sediment uranium	10 km/10 km/−	0.0470	0.0152
Laurentian metasedimentary and volcanics	unit	sediment uranium/alkalinity	5 km/2 km/135	0.2661	1.42×10^{-17}
Piedmont zone Eastern Blue Ridge	element	percent	10 km/7.5 km/180	0.0092	1.59×10^{-20}
Grandfather Mountain Window	unit	sediment uranium	10 km/5 km/45	0.5487	6.84×10^{-13}
Carolina zone Raleigh Terrane	element	percent	10 km/2.5 km/135	0.0207	2.79×10^{-15}
Cherryville Pluton	unit	percent	7.5 km/2.5 km/90	0.0251	0.0018
Milton Terrane	unit	groundwater uranium/conductivity	7.5 km/2.5 km/180	0.6666	1.37×10^{-7}
Beech Pluton	unit	groundwater uranium/conductivity	10 km/1 km/90	54.75	4.23×10^{10}
Deep River Basin	element	sediment uranium/conductivity	7.5 km/2.5 km/180	40.48	1.18×10^{-9}
Piedmont zone Tugaloo	element	percent	7.5 km/1 km/135	0.0135	4.27×10^{11}
Late Paleozoic Plutons	element	percent	5 km/5 km/−	0.0181	3.90×10^{-29}
Henderson Gneiss	unit	percent	10 km/7.5 km/135	0.0300	3.79×10^{-25}
Mecklenburg Pluton	unit	groundwater uranium/conductivity	7.5 km/2.5 km/90	2.814	3.67×10^{-6}
Piedmont zone Eastern Blue Ridge Plutons	element	percent	5 km/2.5 km/90	0.0089	3.73×10^{-6}
Piedmont zone Cat Square Terrane Plutons	element	percent	7.5 km/2.5 km/180	0.0262	5.31×10^{-5}

validation (LOOCV).[28,32] In LOOCV, each log-^{222}Rn value Z_j is removed one at a time, and re-estimated using the given model based only on the remaining data. We assess the accuracy and precision with the root mean squared error (RMSE), the precision with R^2, and the bias of the estimated standard deviation with the root mean squared standardized error (RMSS). Let $Z^{*(k)}$ be the re-estimate for method k, then $\mathrm{RMSE}^{(k)} = [1/n(\sum_{j=1}^{n}(Z_j^{*(k)} - Z_j)^2)]^{1/2}$, the cross-validation R-squared is $R^2(\mathbf{Z}, \mathbf{Z}^{*(k)})$, and the $\mathrm{RMSE}^{(k)} = [1/n(\sum_{j=1}^{n}(Z_j^{*(k)} - Z_j)^2)/\hat{\sigma}_j^{*(k)}]^{1/2}$, where $\hat{\sigma}_j^{*(k)}$ is the prediction standard error. RMSS should be close to one if the prediction standard errors are valid.

2.5. Kruskal–Wallis Hypothesis Tests for LUR model results. A major goal of this study is to help elucidate geologic associations (i.e., intrageological differences) that result in local groundwater ^{222}Rn variability; or to explain anomalies in which a general geological description is associated with elevated ^{222}Rn but contains an element or unit that is associated with low ^{222}Rn. The geology and uranium based explanatory variables and the geological classification scales allow us to generate and test hypotheses from our LUR model results. To this end, we perform a Kruskal–Wallis nonparametric ANOVA test[44] on the ^{238}U or ^{222}Rn concentrations within geological formations that were selected to the final LUR model. For instance, if a general classification scale variable is selected with a geology and uranium based variable and there is an element or unit that is a subset of the general variable with low observed ^{222}Rn concentrations, then we can compare the distributions of the ^{238}U concentrations within the subset geological formation to the larger group, to statistically test if the ^{238}U is significantly higher in the larger group then the subset, thereby driving the larger group's intrageological ^{222}Rn variability. Similarly, we can compare ^{222}Rn distributions in geological formations and their subset formations if both were selected (i.e., element vs general), testing whether subset formations contribute ^{222}Rn concentrations to groundwater in the larger group to varying degrees. The Kruskal–Wallis does not make an assumption on the normality of the data, and the null hypothesis is that the two groups come from the same distribution with equal medians.

3. RESULTS

3.1. Land Use Regression. The results including the geological scale, ^{238}U concentrations, ellipse size and angles, linear coefficients, and p-values of the LUR model selected by ADDRESS for groundwater ^{222}Rn are summarized in Table 1. With 15 explanatory variables selected plus an intercept, the model obtained a R^2 of 0.33 (Pearson correlation coefficient = 0.57). The LUR maps of predicted ^{222}Rn median (geometric mean) and variance are available in the Supporting Information.

3.2. Spatial Covariance Analysis. The purely BME analysis, with an offset of the global log-^{222}Rn mean, was modeled using an anisotropic covariance model with an additive two exponential covariance model for the Blue Ridge and Piedmont physiographic regions, where northeast trending geologic formations result in anisotropic conditions, and an isotropic additive two exponential covariance model for the coastal plains region, where sand and gravel geology result in overall isotropic conditions. Significant differences between the sill (i.e., total variance) and covariance range were found between physiographic regions, which justifies using separate covariance models by region. Additionally, the covariance range differed significantly for the Blue Ridge and Piedmont regions. The model parameters shown below were fit with a least-squared approach:

$$C_X(r) = c_1 \exp\left(-\frac{3r}{a_{r_1}}\right) + c_2 \exp\left(-\frac{3r}{a_{r_2}}\right) \quad (6)$$

where the first component of the sill, c_1 = 1.31, 1.46, and 1.52 $(\log - (\mathrm{pCi/L}))^2$ for the Blue Ridge, Piedmont, and Coastal Plain physiographic regions, respectively; the first spatial covariance range, a_{r_1} = 1,170, 767, and 1113 m for the three physiographic regions respectively; the second component of the sill, c_2 = 0.52, 0.70, and 0.089 $(\log - (\mathrm{pCi/L}))^2$ for the three physiographic regions respectively; and the second spatial covariance range, a_{r_2} = 206, 77, and 2399 km, respectively. The principal axes of anisotropy are 45° and 90° for the Blue Ridge and Piedmont physiographic regions, respectively. The BME covariance model plots and rose diagrams are available in the Supporting Information.

The LUR-BME residual covariance lacks anisotropy in all three physiographic regions (see the Supporting Information),

DOI: 10.1021/acs.est.5b01503
Environ. Sci. Technol. 2015, 49, 9817–9825

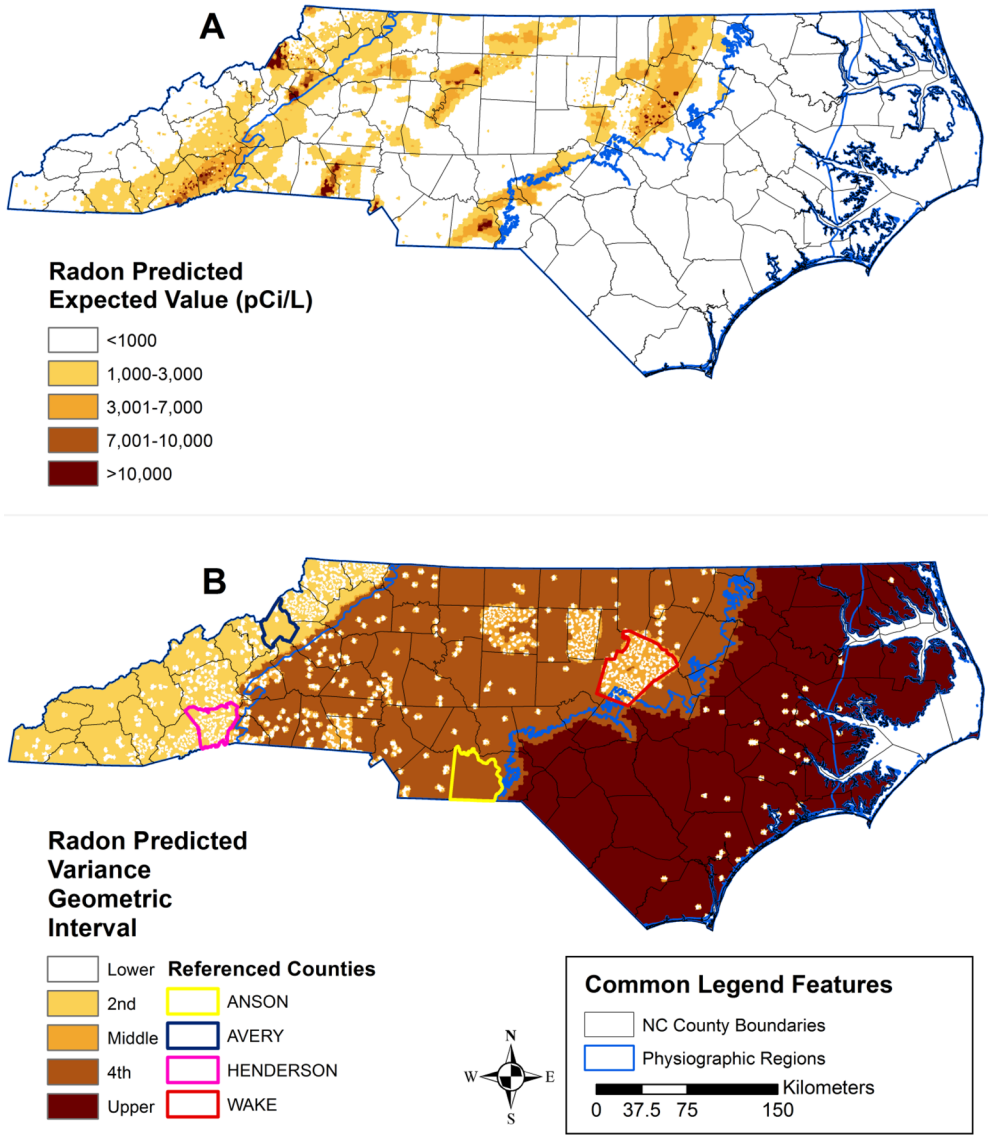

Figure 3. (A) LUR-BME radon predicted median across North Carolina. (B) LUR-BME predicted variance binned according to five geometric intervals. Geometric intervals are roughly quintiles but produce better visualization for non-normal distributions. The counties highlighted in 3B are referenced as discussion points in the main manuscript text in section 4.1. Radon geometric variances are from 1 to 4.6 $(\text{pCi/L})^2$ (0.037−0.17 $(\text{Bq/L})^2$).

likely due to the elliptical based variables in the LUR model successfully capturing the anisotropy. The model parameters for the LUR-BME residual covariance are also fit with a least-squared approach and are detailed as follows: c_1 = 1.31, 1.37, and 1.46 $(\log - (\text{pCi/L}))^2$ for the Blue Ridge, Piedmont, and Coastal Plain physiographic regions, respectively; the first spatial covariance range, a_{r_1} = 881, 1,117, and 1113 m for the three physiographic regions respectively; the Blue Ridge physiographic is a one component exponential model; the second component of the sill, c_2 = 0.11 and 0.07 $(\log - (\text{pCi/L}))^2$ for the Piedmont and Coastal Plain physiographic regions respectively; and the second spatial covariance range, a_{r_2} = 14.96 and 14.98 km, respectively. The covariance ranges for the LUR-BME are significantly shorter than BME alone since the LUR offset capture regional or long-range trends (see the Supporting Information).

3.3. Land Use Regression—Bayesian Maximum Entropy. The LUR model was integrated as the global offset to create a LUR-BME model, which resulted in a LOOCV R^2 of 0.46 (Pearson correlation coefficient = 0.68; Supporting Information Figure S15), a 28% improvement over LUR, and a 4% improvement over BME, which obtained a R^2 of 0.44 (correlation = 0.66). Figure 3 maps the point-level groundwater ^{222}Rn median concentration and variance across North Carolina. The cross-validation results for the LUR, BME, and LUR-BME models are summarized in Table 2.

3.4. Kruskal−Wallis ANOVA. The first variable selected in the final LUR model was the mean sediment ^{238}U within the Intrusive Felsic general geological formations, which contains many geological units known to have elevated groundwater ^{222}Rn. However, the *Greensboro Intrusive Suite* is an intrusive felsic unit that has low groundwater ^{222}Rn levels. In order to explore why the Greensboro Intrusive Suite unit has different ^{222}Rn levels than its parent intrusive felsic formation, we performed a Kruskal−Wallis ANOVA test on the distributions of sediment ^{238}U within the Greensboro Intrusive Suite versus

DOI: 10.1021/acs.est.5b01503
Environ. Sci. Technol. 2015, 49, 9817−9825

Table 2. Leave-One-Out Cross-Validation Statistics for the LUR, BME, and LUR-BME Methods for Estimation of Point-Level log-^{222}Rn[a]

method	RMSE	R^2	RMSS
LUR	1.20	0.33	0.82
BME	1.01	0.44	1.22
LUR-BME	0.99	0.46	1.20

[a]Equations for validation statistics are in section 2.4. RMSE is root mean squared error; R^2 is the coefficient of determination; and RMSS is the root mean squared standardized error. Units for RMSE = (log − (pCi/L)); R^2, RMSS = unitless.

the rest of the intrusive felsic geology. The null hypothesis is rejected with a p-value < 0.001, demonstrating significant difference in the distribution of sediment uranium ^{238}U between the Greensboro Intrusive Suite and other intrusive felsic geologies.

The unit scale Henderson Gneiss, also classified as intrusive felsic, was selected to the final LUR model as a percent geology variable. A Kruskal−Wallis ANOVA test of observed ^{222}Rn distributions within Henderson Gneiss versus other intrusive felsic was rejected with a p-value < 0.001, indicating an underlying higher distribution of ^{222}Rn within subcategories of intrusive felsic geology such as Henderson Gneiss.

4. DISCUSSION

4.1. Groundwater Radon Maps. This study presents a LUR model for point-level ^{222}Rn concentration across North Carolina that elucidates geological and chemical sources affecting its variability, and then utilizes the strengths of BME to create the first map of point-level ^{222}Rn concentrations (R^2 = 0.46) and its prediction uncertainty (RMSS = 1.20). Several major findings can be deduced from the first point-level groundwater ^{222}Rn maps of concentration and uncertainty across North Carolina. First, several areas of high susceptibility to elevated ^{222}Rn as determined by others[15,16,21,45] are confirmed, including the areas underlain by Henderson Gneiss (Henderson County (pink outline Figure 3B); Blue Ridge physiographic region) and Rolesville Batholith (unit subset of Late Paleozoic Plutons; Eastern Wake County (red outline Figure 3B); Piedmont physiographic region). Second, the uncertainty is the highest in the Coastal Plain physiographic region due to the lack of data and thus the highest total variance (i.e., sill, $c_1 + c_2$ in eq 6) out of all three physiographic regions; however, there is no area within the Coastal Plain with a predicted median above 3000 pCi/L (111 Bq/L). This may suggest a lower priority for radon sampling compared to the priority in other regions of the state with higher predicted groundwater radon values. Third, it may be prudent to allocate limited resources for increased monitoring in the Piedmont physiographic region in areas underlain by the Deep River basin (element) and Late Paleozoic Plutons (element) (see the element map in the Supporting Information). Our map is the first to predict (Figure 3A) elevated ^{222}Rn above 3000 pCi/L almost ubiquitously across the Deep River basin and some areas above 10 000 pCi/L (370 Bq/L) in Anson County (yellow outline Figure 3B) due to its inclusion as an explanatory variable. However, these predictions have high uncertainty (Figure 3B) and are underlaid with explanatory variables that greatly exceeded values used in the calibration of the model. For instance, the maximum value of the Deep River Basin variable (conductivity normalized sediment ^{238}U) used in calibration was 0.05 ppb/($\mu\Omega$/(cm)) whereas the maximum value found in the extrapolation of the LUR model was 0.72 ppb/($\mu\Omega$/(cm)). We limited the maximum value of explanatory variables in extrapolated regions to the maximum of the calibration range due to the many orders of magnitude that some explanatory variables cover; nonetheless, high values are predicted due to the large value of its linear regression coefficient (Table 1). Fourth, our map predicts new areas in the Blue Ridge physiographic region with elevated groundwater ^{222}Rn including areas underlain by the Beech Pluton (Avery County, dark blue outline Figure 3B; unit) and Grandfather Mountain Window (unit). The Beech Pluton is also an intrusive felsic formation, which is known to be associated with elevated groundwater ^{222}Rn; however, the likely reason both units were selected in the model was their vicinity to high monitoring values in areas outside their spatial range. The Beech Pluton itself only has one monitoring value within its area; however, 16 monitoring locations with high values are north and hence the Beech Pluton was selected as a long, thin ellipse with a 90° azimuth.

4.2. LUR Model Interpretations. Our LUR-BME model was the first geostatistical model to account for geometric anisotropy of a groundwater contaminant through a LUR model. Our LUR model can be thought of as a groundwater version of Saito and Goovaerts[46] Kriging model for cadmium in air using predominant wind direction as an LUR variable that accounts for geometric anisotropy.

The LUR model sheds light on important variables associated with groundwater ^{222}Rn through the model selection process; however, a lack of selection does not necessarily preclude a variable from an association with groundwater ^{222}Rn. Messier et al.[32] showed with a 10-fold cross-validation that LUR model selection procedures are robust for some selected variables, but other variables may not be due to physical factors like local variability and statistical factors like collinearity with other potential variables. Unit variables selected such as the Beech Pluton may not be robust to a significant change in monitoring data; however, in our model they are all highly significant (Table 1) and removing them from the model results in at least a 4% reduction in the LUR-BME R-squared. The LUR model also allows comparison and distinction between scales of geological formations. For instance, we found the general geological descriptions of intrusive felsic to be important via its selection to the final model; moreover, Henderson Gneiss, Cherryville Pluton, and Beech Pluton are more detailed geologic units that are also intrusive felsic selected to the final model. The linear, additive formulation of the LUR model allowed intrusive felsic to be included and provide a baseline for elevated ^{222}Rn levels across much of North Carolina, which is then refined by units with varying local effects based on their coefficient values. Additionally, the element scale variable Late Paleozoic Plutons and Piedmont zone Eastern Blue Ridge Plutons were selected, which are also at least partly intrusive felsic. Lastly, the difference in scales allows for more significant extrapolation of potential elevated ^{222}Rn areas that may have otherwise been missed. For example, Late Paleozoic Pluton was selected, which contains the unit of elevated ^{222}Rn in Eastern Wake County known as the Rolesville Batholith. If Rolesville Batholith was selected instead of Late Paleozoic Plutons, then there would be less extrapolated high values; but given the selection of Late Paleozoic Plutons, areas in Anson County and Northwestern Guilford County also have higher predicted values and thus identified as areas that may

DOI: 10.1021/acs.est.5b01503
Environ. Sci. Technol. 2015, 49, 9817−9825

benefit from additional groundwater ^{222}Rn sampling. This information can provide useful guidance on selecting and prioritizing areas for new monitoring.

4.3. Associations within Radon Anomalies. The primary mechanisms that release uranium and radon to water are different because of differences in half-life, solubility, and geochemical reactivity of these elements, which determine uranium and radon concentrations in groundwater. Moreover, near-surface chemical weathering mechanisms[47] could cause local spatiotemporal variability in groundwater ^{222}Rn and ^{238}U. Therefore, groundwater ^{238}U is not always an optimal surrogate for groundwater ^{222}Rn concentration, at times not even in areas of uranium-rich granite bedrock,[48,49] which creates apparent anomalies or an unexpected lack of correlation. Our LUR model selection process, with multiple geological formation specific bedrock ^{238}U surrogate variables, helps guide appropriate hypothesis tests to evaluate factors associated with geological radon anomalies. For instance, Campbell et al.[16] and Vinson et al.[45] both noted positive associations between elevated ^{222}Rn and intrusive felsic formations; however, Campbell et al. notes the apparent anomaly of the Greensboro Intrusive Suite, which has low levels of groundwater ^{222}Rn despite being intrusive felsic. The Kruskal−Wallis ANOVA null-hypothesis between sediment ^{238}U was rejected, which means there is significant difference between the distributions of sediment ^{238}U within intrusive felsic formations with elevated ^{222}Rn and intrusive felsic formations with low ^{222}Rn, thus variability of groundwater ^{222}Rn within intrusive felsic formations is likely associated with average bedrock ^{238}U concentrations as defined by sediment ^{238}U concentrations. This is supported by Vinson et al.[45] from data in the Rolesville Batholith, an intrusive felsic formation, which they report has groundwater ^{238}U concentrations 1−2 orders of magnitude higher than surrounding geology and by Yang et al.[48] which found intermediate scale associations between groundwater ^{238}U and ^{222}Rn within granitic plutons.

4.4. Recommendations and Limitations. This study presents a novel method whose result is a point-level mapping with physical interpretations. Human health related recommendations based on the results should however consider the limitations of the study. The results of this study can be used as the exposure assessment in a retrospective epidemiological analysis as this represents the best estimate currently available for groundwater ^{222}Rn concentrations in North Carolina; but, there is the potential for exposure misclassification, especially in areas far away from monitoring data. We recommend that the map of monitoring locations and prediction variance be used in conjunction with predicted expected value for decision-making purposes. Nonetheless, the LUR-BME provides better estimates outside of the spatial covariance range of monitoring locations due to the informed offset based on the LUR (see the Supporting Information; Figure S16). Moreover, LUR-BME also provides the benefit of an accurate quantification of uncertainty (RMSS = 1.20) to use in a risk assessment framework.

The theoretical lower limit of the scale of our LUR estimates is based on 1:1 500 000 map scale geological information used in the study,[33] which results in a theoretical lower limit for detectable size of 1500 m and a raster grid cell size of 750 m.[50] However, when integrated into the BME framework with a point-level groundwater ^{222}Rn data, the mixed-scale LUR-BME method can provide estimates at the point-level. The LUR-BME method presented in this paper is also easily translatable to smaller areas. For instance, the USGS creates geological "Quadrangle" maps at the 1:24 000 map scale, which would allow fine scale geological controls to be resolved given sufficient monitoring data as well. We considered using the 1:24 000 quadrangle maps for this study, but they do not cover the entire study domain, and the level of detail is too refined which results in a majority of zeroes or null explanatory variables. Nonetheless, given sufficient groundwater ^{222}Rn samples in a local area, the quadrangle maps could be used with our method to model point-level variability and elucidate local scale effects of geology.

Groundwater ^{222}Rn has been shown to be positively correlated (R^2 = 0.37) with well and casing depth,[45] but this information was only available for a small subset of our data (<10%). Neither casing nor well depth were considered as potential explanatory variables; however, given that the geological information is also two-dimensional, depth information would not elucidate additional geological controls.

■ ASSOCIATED CONTENT

Supporting Information

The Supporting Information is available free of charge on the ACS Publications website at DOI: 10.1021/acs.est.5b01503.

Radon data sources, maps of based on Hibbard et al.[33] geology data by geological scale, Figures S1−S16, LUR explanatory variables summary, BME rose diagrams, re-estimation with increasing distance to nearest neighbor, and further references (PDF)

■ AUTHOR INFORMATION

Corresponding Author

*Mailing Address: 1303 Michael Hooker Research Center, Chapel Hill, NC 27599. E-mail: kmessier@live.unc.edu. Phone: (919) 966-1095. Fax: (919) 966-7911.

Notes

The authors declare no competing financial interest.

■ ACKNOWLEDGMENTS

This research was supported in part by funds from the NIH T32ES007018, NIOSH 2T42OH008673, and North Carolina Water Resources Research Institute (WRRI) project number 11-05-W.

■ REFERENCES

(1) WHO. *WHO guidelines for drinking-water quality*; 2011.

(2) Darby, S.; Hill, D.; Auvinen, A.; Barros-Dios, J. M.; Baysson, H.; Bochicchio, F.; Deo, H.; Falk, R.; Forastiere, F.; Hakama, M.; et al. Radon in homes and risk of lung cancer: collaborative analysis of individual data from 13 European case-control studies. *BMJ* **2005**, *330*, 223.

(3) Field, R. W.; Smith, B.; Steck, D.; Lynch, C. F. Residential radon exposure and lung cancer: variation in risk estimates using alternative exposure scenarios. *J. Exposure Anal. Environ. Epidemiol.* **2002**, *12*, 197−203.

(4) Kendall, G. M.; Smith, T. J. Doses to organs and tissues from radon and its decay products. *J. Radiol. Prot.* **2002**, *22*, 389−406.

(5) Lubin, J. H.; Boice, J. D. Lung cancer risk from residential radon: meta-analysis of eight epidemiologic studies. *J. Natl. Cancer Inst.* **1997**, *89*, 49−57.

(6) Field, R. W. Environmental Factors in Cancer: Radon. *Rev. Environ. Health* **2010**, *25*, 33−38.

(7) Krewski, D.; Lubin, J. H.; Zielinski, J. M.; Alavanja, M.; Catalan, V. S.; Field, R. W.; Klotz, J. B.; Letourneau, E. G.; Lynch, C. F.; Lyon,

DOI: 10.1021/acs.est.5b01503
Environ. Sci. Technol. 2015, 49, 9817−9825

J. I.; et al. Residential Radon and Risk of Lung Cancer. *Epidemiology* **2005**, *16*, 137−145.
(8) USEPA. http://www.epa.gov/radon/healthrisks.html (accessed June 1st, 2014).
(9) National Research Council. *Risk Assessment of Radon in Drinking Water*; Washington D.C, 1999.
(10) Vinson, D. S.; Campbell, T. R.; Vengosh, A. Radon transfer from groundwater used in showers to indoor air. *Appl. Geochem.* **2008**, *23*, 2676−2685.
(11) Fitzgerald, B.; Hopke, P. K. Experimental Assessment of the Short- and Long-Term Effects of Rn from Domestic Shower Water on the Dose Burden Incurred in Normally Occupied Homes. *Environ. Sci. Technol.* **1997**, *31*, 1822−1829.
(12) Auvinen, A.; Salonen, L.; Pekkanen, J.; Pukkala, E.; Ilus, T.; Kurttio, P. Radon and other natural radionuclides in drinking water and risk of stomach cancer: a case-cohort study in Finland. *Int. J. Cancer* **2005**, *114*, 109−113.
(13) Brutsaert, W. F.; Norton, S. A.; Hess, C. T.; Williams, J. S. Geologic and Hydrologic Factors Controlling Radon-222 in Ground Water in Maine. *Groundwater* **1981**, *19*, 407−417.
(14) Yang, Q.; Smitherman, P. E.; Hess, C. T.; Culbertson, C. W.; Marvinney, R. G.; Smith, A. E.; Zheng, Y. Uranium and radon in private bedrock well water in Maine: geospatial analysis at two scales. *Environ. Sci. Technol.* **2014**, *48*, 4298−4306.
(15) Loomis, D. P. Radon-222 Concentration and Aquifer Lithology in North Carolina. *Groundwater Monit. Rem.* **1987**, *7*, 33−39.
(16) Campbell, T.; Mort, S.; Fong, F.; Crawford-Brown, D.; Vengosh, A.; Cornell, E.; Field, W. R. *North Carolina Radon-in-Water Advisory Committee Report*; Raleigh, North Carolina, 2011.
(17) Zhu, H. C.; Charlet, J. M.; Doremus, P. Kriging Radon Concentration of Groundwaters in Western Ardennes. *Environmetrics* **1996**, *7*, 513−523.
(18) Skeppström, K.; Olofsson, B. A prediction method for radon in groundwater using GIS and multivariate statistics. *Sci. Total Environ.* **2006**, *367*, 666−680.
(19) Salih, I. M.; Pettersson, H. B. L.; Sivertun, A.; Lund, E. Spatial correlation between radon (222-Rn) in groundwater and bedrock uranium (238-U): GIS and geostatistical analyses. *J. Spat. Hydrol.* **2002**, *2* (2), 1−10.
(20) US Environmental Protection Agency. EPA Map of Radon Zones. http://www.epa.gov/radon/zonemap.html (accessed June 1st, 2014).
(21) Gundersen, L. C. S.; Schumann, R. R.; White, S. W. *Geologic Radon Potential of EPA Region 4: Alabama, Florida, Georgia, Kentucky, Mississippi, North Carolina, South Carolina, Tennessee*; 1993; Open-File Report 93-292-D.
(22) USEPA. http://water.epa.gov/lawsregs/rulesregs/sdwa/index.cfm (accessed February 12th, 2015).
(23) Kenny, J. F.; Barber, N. L.; Hutson, S. S.; Linsey, K. S.; Lovelace, J. K.; Maupin, M. A. *Estimated Use of Water in the United States in 2005*; U.S. Geological Survey: Reston, VA, 2009; Circulation 1344.
(24) Nolan, B. T.; Hitt, K. J. Vulnerability of shallow groundwater and drinking-water wells to nitrate in the United States. *Environ. Sci. Technol.* **2006**, *40*, 7834−7840.
(25) Su, J. G.; Jerrett, M.; Beckerman, B. A distance-decay variable selection strategy for land use regression modeling of ambient air pollution exposures. *Sci. Total Environ.* **2009**, *407*, 3890−3898.
(26) Nuckols, J. R.; Beane Freeman, L. E.; Lubin, J. H.; Airola, M. S.; Baris, D.; Ayotte, J. D.; Taylor, A.; Paulu, C.; Karagas, M. R.; Colt, J.; et al. Estimating Water Supply Arsenic Levels in the New England Bladder Cancer Study. *Environ. Health Perspect.* **2011**, *119*, 1279.
(27) Kim, D.; Miranda, M. L.; Tootoo, J.; Bradley, P.; Gelfand, A. E. Spatial Modeling for Groundwater Arsenic Levels in North Carolina. *Environ. Sci. Technol.* **2011**, *45*, 4824−4831.
(28) Messier, K. P.; Akita, Y.; Serre, M. L. Integrating address geocoding, land use regression, and spatiotemporal geostatistical estimation for groundwater tetrachloroethylene. *Environ. Sci. Technol.* **2012**, *46*, 2772−2780.
(29) Rodríguez-Lado, L.; Sun, G.; Berg, M.; Zhang, Q.; Xue, H.; Zheng, Q.; Johnson, C. A. Groundwater arsenic contamination throughout China. *Science* **2013**, *341*, 866−868.
(30) Christakos, G.; Li, X. Bayesian Maximum Entropy Analysis and Mapping: A Farewell to Kriging Estimators ? *Math. Geol.* **1998**, *30*, 435−462.
(31) Sanders, A. P.; Messier, K. P.; Shehee, M.; Rudo, K.; Serre, M. L.; Fry, R. C. Arsenic in North Carolina: public health implications. *Environ. Int.* **2012**, *38*, 10−16.
(32) Messier, K. P.; Kane, E.; Serre, M. L. *Environ. Sci. Technol.* **2014**, *48*, 10804.
(33) Hibbard, J.; van Stall, C.; Rankin, D.; Williams, H. *Lithotectonic Map of Appalachian Orogen: Canada-United States of America*; Geological Survey of Canada, 2006; Map 0206A, map scale 1:1 500 000.
(34) *National Uranium Resource Evaluation (NURE) Hydrogeochemical and Stream Sediment Reconnaissance data*; U.S. Geological Survey: Denver, CO, 2004.
(35) Kinner, N. E.; Malley, J. P., Jr.; Clement, J. A.; Quern, P. A.; Schell, G. S.; Lessard, C. E. Effects of Sampling Technique, Storage, Cocktails, Sources of Variation, and Extraction on the Liquid Scintillation Technique for Radon in Water. *Environ. Sci. Technol.* **1991**, *25*, 1165−1171.
(36) Hahn, P. B.; Pia, S. H. *Determination of Radon in Drinking Water by Liquid Scintillation Counting*; USEPA: Las Vegas, NV, 1991.
(37) Messier, K. P.; Kane, E.; Bolich, R.; Serre, M. L. Nitrate Variability in Groundwater of North Carolina using Monitoring and Private Well Data Models. *Environ. Sci. Technol.* **2014**, *48*, 10804−10812.
(38) Wanty, R. B.; Lawrence, E. P.; Gundersen, L. C. S. A theoretical model for the flux of radon from rock to ground water. *Geol. Soc. Am. Spec. Pap.* **1992**, *271*, 73−78.
(39) Dall'Aglio, M. Planning and interpretation criteria in hydrogeochemical prospecting for uranium. In *Uranium Prospecting Handbook*; Bowie, S. H. U., Davis, M., Ostle, D., Eds.; The Institution of Mining and Metallurgy, 1972; pp 121−134.
(40) Wenrich-Verbeek, K. J. *Geochemical Exploration for Uranium Utilizing Water and Stream Sediments*; United States Department of the Interior Geological Survey, 1980
(41) Christakos, G. A Bayesian/maximum-entropy view to the spatial estimation problem. *Math. Geol.* **1990**, *22*, 763−777.
(42) Serre, M. L.; Christakos, G. Modern geostatistics: computational BME analysis in the light of uncertain physical knowledge - the Equus Beds study. *Stoch. Environ. Res. Risk Assess.* **1999**, *13*, 1−26.
(43) Christakos, G.; Bogaert, P.; Serre, M. L. *Temporal GIS: Advanced Function for Field-Based Applications*; Springer: New York, NY, 2002.
(44) Kruskal, W. H.; Wallis, W. A. Use of Ranks in One-Criterion Variance Analysis. *J. Am. Stat. Assoc.* **1952**, *47*, 583−621.
(45) Vinson, D. S.; Vengosh, A.; Hirschfeld, D.; Dwyer, G. S. Relationships between radium and radon occurrence and hydrochemistry in fresh groundwater from fractured crystalline rocks, North Carolina (USA). *Chem. Geol.* **2009**, *260*, 159−171.
(46) Saito, H.; Goovaerts, P. Accounting for source location and transport direction into geostatistical prediction of contaminants. *Environ. Sci. Technol.* **2001**, *35*, 4823−4829.
(47) Guthrie, V. A.; Kleeman, J. D. Changing uranium distributions during weathering of granite. *Chem. Geol.* **1986**, *54*, 113−126.
(48) Yang, Q.; Smitherman, P. E.; Hess, C. T.; Culbertson, C. W.; Marvinney, R. G.; Smith, A. E.; Zheng, Y. Uranium and radon in private bedrock well water in Maine: geospatial analysis at two scales. *Environ. Sci. Technol.* **2014**, *48*, 4298.
(49) Chapman, M. J.; Cravotta, C. A.; Szabo, Z.; Lindsey, B. D. *Naturally Occurring Contaminants in the Piedmont and Blue Ridge Crystalline-Rock Aquifers and Piedmont Early Mesozoic Basin Siliciclastic-Rock Aquifers, Eastern United States*; U.S. Geological Survey: Reston, VA, 2013; Scientific Investigations Report 2013−5072, p 74.
(50) Tobler, W. Measuring Spatial Resolution. In *Land Resources Information Systems Conference*; Beijng, China, 1988; pp 12−16.

DOI: 10.1021/acs.est.5b01503
Environ. Sci. Technol. 2015, 49, 9817−9825